An All-Passive Negative Feedback Network for Broadband and Wide Field-of-View Self-Steering Beam-Forming With Zero DC Power Consumption

Min-Yu Huang, *Student Member, IEEE*, Taiyun Chi, *Student Member, IEEE*, Fei Wang, *Student Member, IEEE*, and Hua Wang, *Senior Member, IEEE*

***Abstract*— This paper presents an all-passive negative feedback network that performs autonomous radio-frequency (RF) front-end beam-forming and dynamic beam-tracking toward the direction of the incident RF signal. The proposed feedback network consists of a passive RF signal processing network, voltage rectifiers, and voltage-controlled delay-line phased shifters, all of which are passive-only circuits. The negative feedback loop is realized by passive phase detection, phase-to-voltage conversion, and voltage-controlled phase shifting, achieving a large loop-gain and autonomous operation with zero DC power consumption. The nonlinear behavior of the loop is exploited to substantially expand the array field of view (FoV). A proof-of-concept broadband four-element all-passive self-steering beam-former at 5 GHz with a wide FoV is implemented in a standard 130 nm CMOS process. A high-quality four-element synthesized array factor is measured for the input progressive phase shift ϕ_{in} from $-180°$ to $180°$. When the proposed negative feedback loop is enabled, the normalized array factor is $-2.87/-2.8$ dB at $\phi_{in} = +90°/-90°$ with an input RF power P_{in} of -17 dBm/element at 5 GHz, achieving >25 dB array factor improvement over the open-loop operation. Moreover, the nonlinear feedback loop allows for significant array factor improvement even at $\phi_{in} = +180°/-180°$. The proposed beam-former also achieves high-quality self-steering beam-forming from 4 to 5.68 GHz with 34.7% fractional bandwidth. Therefore, the proof-of-concept all-passive self-steering beam-former outperforms the state-of-the-art active designs in terms of beam-forming quality, FoV, and fractional bandwidth. To the best of the authors' knowledge, this is the first demonstration of an all-passive negative feedback network for a broadband and wide FoV self-steering beam-forming with zero DC power consumption.**

***Index Terms*— Adaptive phased array, beam-forming, energy harvesting, field of view (FoV), low-power wireless, negative feedback, passive network, retro-directive array, self-powered network, self-steering, sensing network.**

Manuscript received August 15, 2016; revised November 3, 2016; accepted December 6, 2016. Date of publication February 14, 2017; date of current version April 20, 2017. This paper was approved by Guest Editor Danilo Manstretta.

The authors are with the Electrical and Computer Engineering Department, Georgia Institute of Technology, Atlanta, GA 30308 USA (e-mail: minyu@gatech.edu; terrychi@gatech.edu; feiwang@gatech.edu; hua.wang@ece.gatech.edu).

Color versions of one or more of the figures in this paper are available online at http://ieeexplore.ieee.org.

Digital Object Identifier 10.1109/JSSC.2016.2641947

I. Introduction

PHASED-array receivers are extensively employed in modern communication and radar systems [1]–[3]. For an N-element uniform receiver array, if the beam is perfectly aligned with the incident wave, the signal-to-noise ratio (SNR) of the receiver array is improved by $10\log N$. However, any beam misalignment in practice will substantially degrade the array SNR and link performance; this is particularly problematic for large-scaled arrays due to their narrow beam widths, e.g., in next-generation 5G links and advanced radars. Conventionally, back-end digital signal processing (DSP) is used to perform array beam-forming and alignment at the expense of extra power consumption, slow response time, and system complexity [4].

Without back-end DSP or manual beam alignment, front-end self-steering beam-formers can automatically track the incident beam [5]–[7]. The self-steering beam-former can benefit numerous applications, such as energy-efficient large-scaled phased array [11], radio-frequency identification [12], low-power sensor network [13], and wireless energy harvesting [14], [15]. A generic system of a self-steering beam-former without any external control is shown in Fig. 1. θ is the incident angle from $-90°$ to $90°$. ϕ_{in} is the input progressive phase shift from $-180°$ to $180°$ in a $\lambda/2$-spaced receiver array, given $\phi_{in} = 180° \times \sin\theta$. The self-steering beam-forming enables fast and accurate system response and reduces the overhead and complexity for generating external open-loop phase-shift controls.

Existing self-steering beam-formers are mostly based on active approaches and consume considerable DC power per array element [5]–[7]. For example, off-chip active phase detectors and active phased shifters are used in [5] to track and compensate the beam alignment with a total DC power of 430 mW. In [6], active power detector and microcontrollers consume a DC power of around 560 mW. Injection-locked oscillator arrays [8], [9] and injection-locked coupled oscillator arrays (COAs) [10] are utilized to autonomously correct the beam misalignment. However, external injection signals and manual alignment are often needed to adjust the beam angle [8]–[10]. Moreover, these oscillator-based systems are

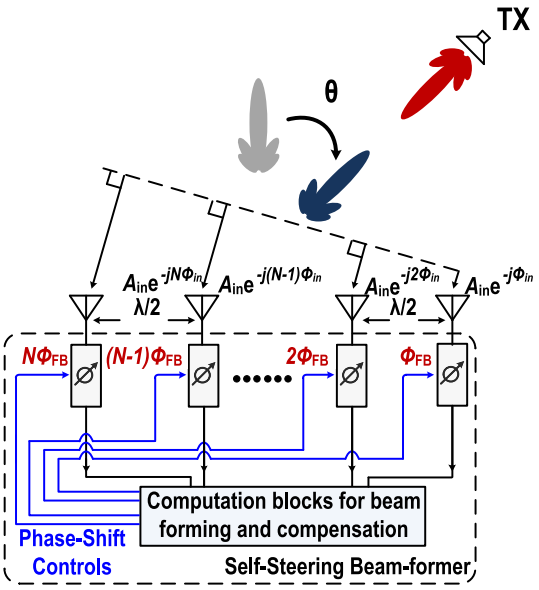

Fig. 1. Conceptual system schematic of a generic self-steering beam-former in a phased-array receiver system.

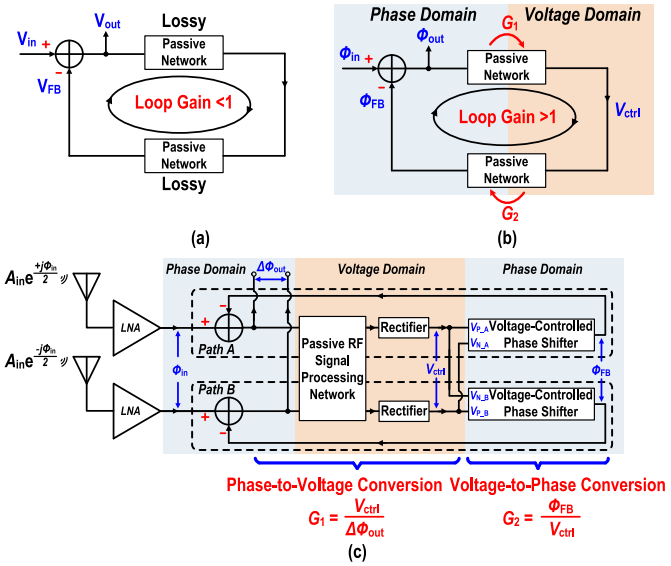

Fig. 2. (a) Conceptual block diagram of an all-passive negative feedback network operating in only one signal domain. (b) Conceptual block diagram of an all-passive negative feedback network operating in phase domain and voltage domain. (c) Simplified schematic of the all-passive negative feedback network for self-steering beam-forming, shown in the phase and voltage signal domains.

often narrowband due to the injection locking nature [8]–[10]. Recently, COAs and coupled phased-lock loops have been used for automatic beam-forming and tracking [7]. Besides substantial DC power consumption and narrow-band operation, these architectures exhibit direct degradation of system stability and field of view (FoV) for large number of array elements, limiting their use in large-scaled array [7]. Therefore, there is an unmet need for accurate, autonomous, and dynamic beam-forming architecture that can operate at the radio-frequency (RF) front-end and support low-power large-scaled phased arrays.

To address these challenges, this paper proposes an all-passive self-steering beam-former using a passive network with negative feedback for automatic, broadband, and wide-FoV beam-forming at the RF front-end [16]. Unlike existing active self-steering beam-formers, the all-passive nature of the proposed design ensures its zero DC operation power, which is critical for large-scaled and/or energy-constrained phased arrays. In addition, compared with energy-harvesting-based systems [17]–[19], the proposed system does not require any energy storage/charging, and it responds instantaneously to the input RF beam and operates continuously without any duty cycle operation. Thus, the receiver can capture the incoming information with no downtime, and there is no need for energy storage element. Moreover, unlike the active approaches, e.g., COAs [7], the all-passive approach ensures no signal re-emission by the beam-former. This electromagnetically "quiet" nature is particularly useful for many military and high-security applications.

As a proof-of-concept demonstration, a broadband and wide-FoV four-element all-passive self-steering beam-former is implemented in a standard 130 nm CMOS process. A high-performance array operation is achieved for the input progressive phase shift ϕ_{in} between $-180°$ and $+180°$ and over an operating frequency range from 4 to 5.68 GHz. At $P_{\text{in}} = -17$ dBm/element, the closed-loop normalized array factor at 5 GHz is measured as $-2.87/-2.8$ dB at ϕ_{in} of $+90°/-90°$, i.e., the array null point without self-steering operation, showing >25 dB array factor improvement over the open-loop operation. The proposed all-passive self-steering beam-former outperforms all the reported active designs for the operation bandwidth, FoV, and beam-forming quality.

This paper is organized as follows. Section II presents the system architecture and operation principle of the all-passive negative feedback network for self-steering beam-forming. The details of a 5 GHz four-element beam-former prototype are discussed in Section III. Section IV shows the measurements and a performance comparison with reported active self-steering beam-formers.

II. All-Passive Network With Negative Feedback for Self-Steering Beam-Forming

A self-steering beam-former should respond autonomously and accurately to the input beam without any external control signal, which therefore requires some negative feedback mechanism in the beam-forming operation. Two conceptual diagrams that connect passive networks and form negative feedback configurations are shown in Fig. 2(a) and (b). Passive networks in practice only exhibit signal loss and cannot provide any power gain due to the conservation of energy. Therefore, if two passive networks are connected in a negative feedback loop and process signals in the same signal domain, e.g., RF power, the overall loop gain is always less than one, which is incapable of producing a desired compensation signal to track the input and reduce the error signal [Fig. 2(a)]. However, in the context of beam-forming/beam-tracking, the progressive and relative phase among the array elements is actually the signal of interest, and such phase information is not directly related with the energy of the RF signals being

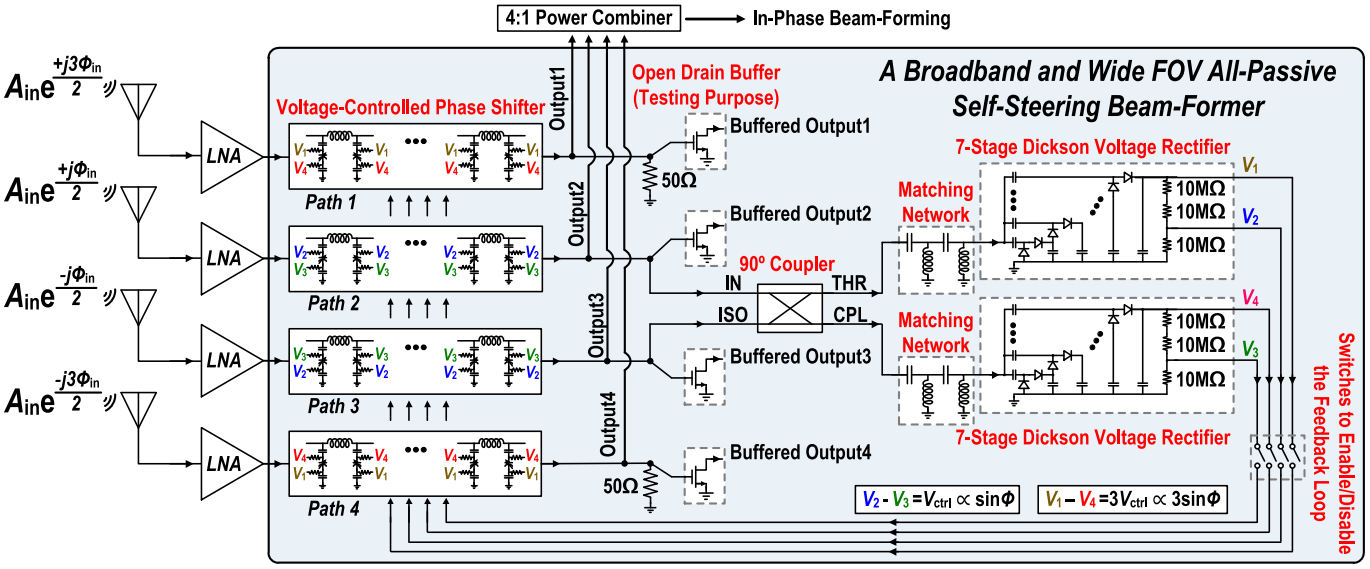

Fig. 3. Top-level circuit schematic of an all-passive broadband and wide-FoV four-element self-steering beam-former in a phased-array receiver. LNAs and 4:1 power combiner are not included in this design.

processed in the array. Moreover, if the forward and feedback passive networks can convert the signals between two signal domains, e.g., phase and voltage, the overall loop gain of such an all-passive negative-feedback networks can be potentially greater than one due to the interdomain signal conversions [Fig. 2(b)]. This concept can be intuitively understood. For example, one can employ multiple voltage-controlled phase shifters in cascade to process the received RF signal, and a small control voltage change can generate a large total phase shift, i.e., achieving a large voltage-to-phase conversion gain, without any external power supply. The proposed all-passive negative feedback network for self-steering beam-forming follows this architecture concept [Fig. 2(c)]. It first detects the phase difference of the incident signal between two array elements by a passive phase detector, yielding a differential phase-dependent voltage output. To complete the negative feedback loop, this voltage signal is then converted back to the phase domain as a differential compensation phase signal by voltage-controlled phase shifters. Note that the passive detectors and the voltage-controlled phase shifters are nonreciprocal networks used to facilitate the proposed negative feedback. The detailed operation principle is explained as follows.

Assume that ϕ_{in} is the progressive phase shift of the RF inputs between two adjacent elements [path A and path B in Fig. 2(c)]. The negative feedback loop generates the phase compensation signal ϕ_{FB} to minimize the residual output phase difference $\Delta\phi_{out}$ and achieve automatic beam alignment of path A and path B. First, the path A/path B residual phase difference $\Delta\phi_{out}$ is transformed to a differential DC voltage V_{ctrl} by a passive RF signal processing network and two rectifiers, which collectively function as a passive phase detector. The large-signal phase-to-voltage conversion gain $G_1 = V_{ctrl}/\Delta\phi_{out}$ can be derived based on the specific circuit implementation. Next, by applying V_{ctrl} on the voltage-controlled phase shifters, the feedback compensation phase

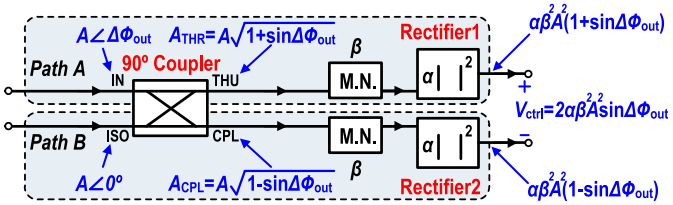

Fig. 4. Passive phase-to-voltage conversion circuit, i.e., a passive phase detector, using a 90° coupler, two matching networks, and two rectifiers.

ϕ_{FB} is generated with a voltage-to-phase conversion gain $G_2 = \phi_{FB} / V_{ctrl}$. The differential V_{ctrl} polarities are selected to ensure an overall negative feedback in the phase domain. Thus, the loop gain is G_1G_2, and the resulting phase error $\Delta\phi_{out}$ as the residual output phase difference is

$$\Delta\phi_{out} = \phi_{in} - \phi_{FB} = \phi_{in}/(1 + G_1G_2). \quad (1)$$

To autonomously and accurately align the receiver beam with the incident signal over a wide FoV, the loop gain G_1G_2 should be maximized over a broad progressive phase shift range ϕ_{in}. This is accomplished by exploiting the nonlinear conversion between the phase and voltage domain and nonlinear operation of the feedback loop, while the entire loop is kept all-passive with zero DC power consumption. Moreover, unlike [7]–[10], the proposed all-passive self-steering beam-former does not require to know the actual frequency of the incident signals *a priori*; this frequency agnostic nature ensures its broadband operation and utility in practical array applications.

III. Circuit Implementation

To demonstrate the proposed all-passive negative feedback network for self-steering beam-forming, a four-element proof-of-concept design at 5 GHz is implemented [16] (Fig. 3). The inner two signal paths (path 2 and path 3) are included in the negative feedback loop, while the outer two paths (path 1 and

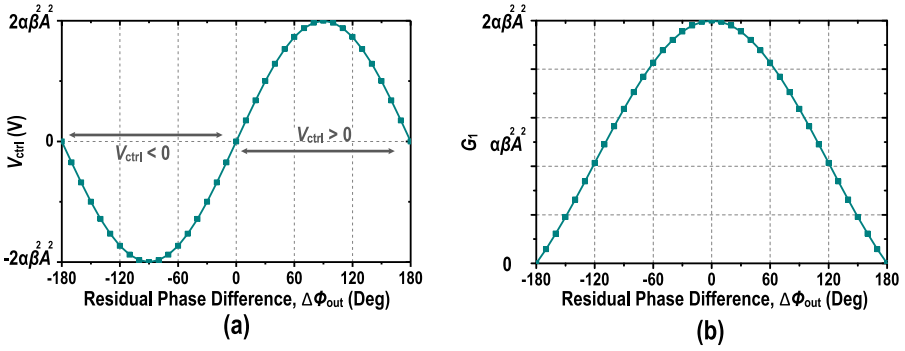

Fig. 5. (a) Differential feedback DC voltage V_{ctrl} versus the residual phase difference $\Delta\phi_{\text{out}}$. (b) Large-signal phase-to-voltage conversion gain G_1 versus the residual phase difference $\Delta\phi_{\text{out}}$.

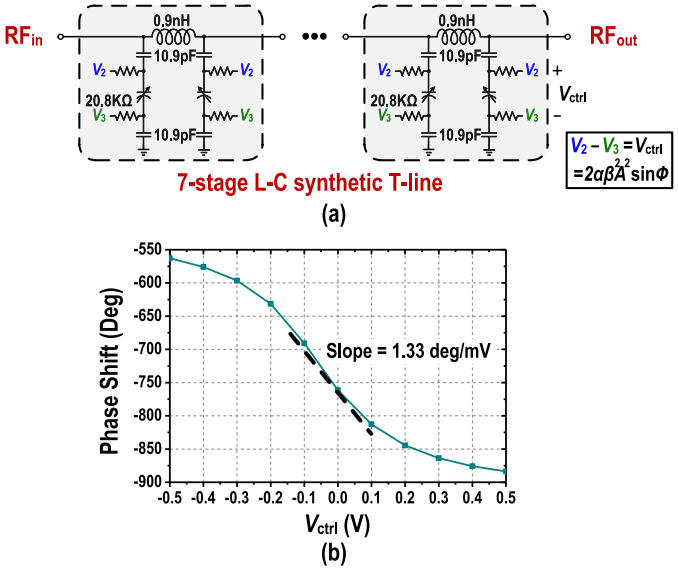

Fig. 6. (a) A seven-stage *LC* synthetic delay line with varactors as the voltage-controlled phase shifter. (b) Simulated phase shift versus differential control voltage V_{ctrl}.

path 4) are controlled in an open-loop manner. This all-passive self-steering beam-former can be employed after front-end low-noise amplifiers (LNAs) in an RF phased-array receiver; additional down-conversion mixers can be added before the beam-former for millimeter-wave operations. Once the receiver is aligned with the incoming beam by the proposed beam-former, the four outputs can be in-phase combined for beam-forming. Four open-drain buffers are used in this proof-of-concept design only to facilitate the testing. Switches are added to enable or disable the feedback loop for open-loop or closed-loop measurements, respectively.

A. Passive Phase-to-Voltage Convertor Analysis

The simplified passive phase-to-voltage convertor is shown in Fig. 4. It consists of a 90° coupler as an RF signal processing network, two matching networks, and two seven-stage Dickson voltage rectifiers [20]. The 90° coupler utilizes an ultracompact transformer-based topology [21], [22] with a characteristic impedance of 50 Ω. The two input signals in path A and path B are concurrently fed to the *input (IN)* and *isolation (ISO)* ports of the 90° coupler. The two resulting outputs from the *through (THR)* and *coupled (CPL)* ports are fed to the Dickson voltage rectifiers. To maximize the driving voltage amplitude for the Dickson voltage rectifiers, two-stage *LC* matching networks are used to down-transform the rectifier input impedance to 50 Ω. The outputs of the rectifiers are then used as the differential control voltages V_{ctrl} to drive the passive voltage-controlled phase shifters to generate the compensation phase ϕ_{FB}. The large-signal behavior of the phase-to-voltage converter can be analyzed by applying two RF incident signals with the same amplitude A but at a phase difference $\Delta\phi_{\text{out}}$ into the *IN* and *ISO* ports of the 90° coupler. The voltage amplitudes of the output RF signals at the *THR* and *CPL* ports are

$$A_{\text{THR}} = \left|\frac{A}{\sqrt{2}}(1 - je^{j\,\Delta\phi_{\text{out}}})\right| = A\sqrt{1+\sin\Delta\phi_{\text{out}}}, \text{ and}$$
$$A_{\text{CPL}} = \left|\frac{A}{\sqrt{2}}(e^{j\,\Delta\phi_{\text{out}}} - j)\right| = A\sqrt{1-\sin\Delta\phi_{\text{out}}}. \quad (2)$$

Thus, the 90° coupler transforms the phase difference of the two RF inputs to the voltage amplitude of the RF outputs, which are further converted to a differential DC voltage V_{ctrl} by the rectifiers. Assume that the matching networks increase the output RF voltage amplitude by a factor of β due to its impedance transformation, and assume that the two matched rectifiers are square-law devices with a conversion coefficient α. The DC output voltages of the two rectifiers are

$$V_{\text{out,rectifier1}} = \alpha\beta^2 A_{\text{THR}}^2 = \alpha\beta^2 A^2(1+\sin\Delta\phi_{\text{out}}), \text{ and} \quad (3)$$
$$V_{\text{out,rectifier2}} = \alpha\beta^2 A_{\text{CPL}}^2 = \alpha\beta^2 A^2(1-\sin\Delta\phi_{\text{out}}). \quad (4)$$

Thus, the differential feedback voltage signal V_{ctrl} is obtained as

$$V_{\text{ctrl}} = V_{\text{out,rectifier1}} - V_{\text{out,rectifier2}} = 2\alpha\beta^2 A^2 \sin\Delta\phi_{\text{out}}. \quad (5)$$

The large-signal open-loop phase-to-voltage conversion gain G_1 can be further calculated as

$$G_1 = V_{\text{ctrl}}/\Delta\phi_{\text{out}} = 2\alpha\beta^2 A^2 \sin\Delta\phi_{\text{out}}/\Delta\phi_{\text{out}}. \quad (6)$$

Fig. 5 plots V_{ctrl} and G_1 versus the residual phase difference $\Delta\phi_{\text{out}}$, i.e., the phase difference between adjacent array elements after the self-steering compensation. G_1 is a sinc function with its peak value at $\Delta\phi_{\text{out}} = 0°$. Its open-loop response gradually decreases to zero when $\Delta\phi_{\text{out}}$ approaches ±180°. Therefore,

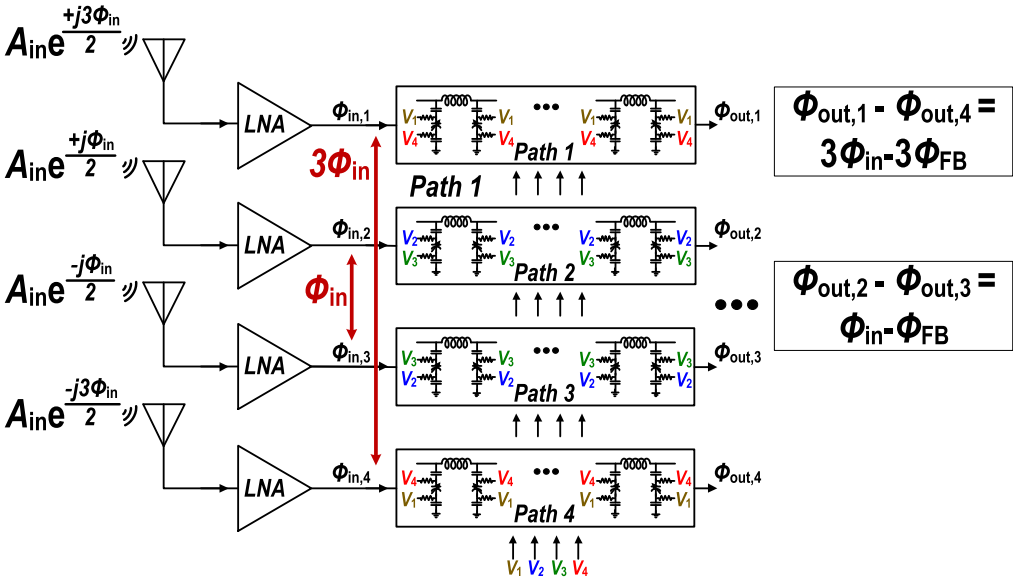

Fig. 7. Input progressive phase shift of path 1 and path 4 (outer two paths) is three times larger than that of path 2 and path 3 (inner two paths). Thus, path 1 and path 4 require $3\phi_{FB}$ for phase compensation and thus $3V_{ctrl}$ as the control voltage.

a positive conversion gain is maintained over the entire ±180° phase shift range.

To achieve a high conversion coefficient α and maximize the phase-to-voltage conversion gain G_1, seven-stage Dickson rectifiers are implemented using zero-threshold transistors (V_{th}~70 mV). In addition, the matching networks scale the coupler's 50 Ω outputs to high impedance values at the rectifiers' inputs, which passively amplifies the RF voltage swings at the rectifier inputs ($\beta > 1$) and further facilitates the rectification. By combining these techniques, the proposed rectification scheme can properly operate with μW-level RF inputs (−17 dBm/path nominal) and provide a significant phase-to-voltage conversion gain G_1 over a wide FoV.

The proposed passive phase-to-voltage convertor serves as a wide-FoV passive phase detector. Unlike active analog multiplier-based phase detector, it extracts the phase difference of two RF signal paths with no DC power consumption. Compared with comparator-based phase detectors, it operates with RF signals at a low detection sensitivity (μW level), which is verified by the measurements and includes circuit noise in practice. Although the phase-to-voltage conversion gain G_1 depends on the input RF amplitude, this does not affect the negative feedback operation for self-steering beamforming, as long as the RF inputs are adequately strong to make the total loop gain G_1G_2 sufficiently larger than one. However, the loop gain gradually degrades at a lower input RF power, which sets the sensitivity limit of the beamformer. Furthermore, just like other self-steering beam-forming circuits, this beam-former should be used in conjunction with front-end blocker rejection circuits, which means that the self-steering beam-former processes only the desired signal. Therefore, the proposed system is considered to process one set of the input signals without considering the effect of blocker signals. The measured and simulated self-steering performance versus the input RF power will be presented and discussed in Section IV.

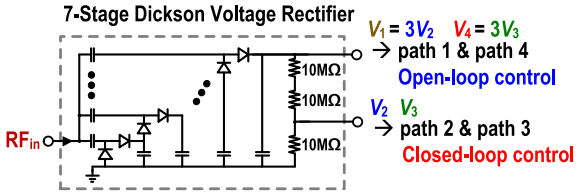

Fig. 8. Seven-stage Dickson voltage rectifier using a 3:1 resistor divider load to generate V_{ctrl} for path 2 (and 3) and $3V_{ctrl}$ for path 1 (and 4). V_2 and V_3 represent the voltages generated by the rectifiers with $V_{ctrl} = V_2$-V_3 (Fig. 3). V_1 and V_4 are their 3× replica voltages with $3V_{ctrl} = V_1$–V_4.

B. Passive Voltage-to-Phase Convertor Analysis

The passive voltage-to-phase convertor, i.e., a voltage-controlled phase shifter, is implemented as a seven-stage *LC* synthetic delay line with varactors in this design [Fig. 6(a)]. The control voltages of the varactors V_2 and V_3 are generated from the two rectifiers. The differential voltage difference of V_2 and V_3 is V_{ctrl}. The simulated phase shift versus V_{ctrl} at 5 GHz is shown in Fig. 6(b). The linear region slope, i.e., the voltage-to-phase conversion gain, is 1.33°/mV at 5 GHz.

The differential DC voltage V_{ctrl} is connected to the varactors in path 2 and path 3 (inner two paths) with opposite polarities to achieve desired differential phase compensation and double the effective voltage-to-phase conversion gain (Fig. 3). The simulated voltage-to-phase differential conversion gain G_2 is $2 \times 1.33°/mV = 2.66°/mV$ at 5 GHz. The averaged loss of the seven-stage *LC* synthetic T-line is 8 dB, which can be compensated by the front-end LNAs. The phase shifter design can adopt wire-bonding inductors and off-chip varactors to further reduce the loss.

C. Open-Loop Controls of the Outer Paths

In a uniform array, the input progressive phase shift of path 1 and path 4 (outer two paths) is three times of path 2 and path 3 (inner two paths) (Fig. 7). Thus, path 1 and path 4

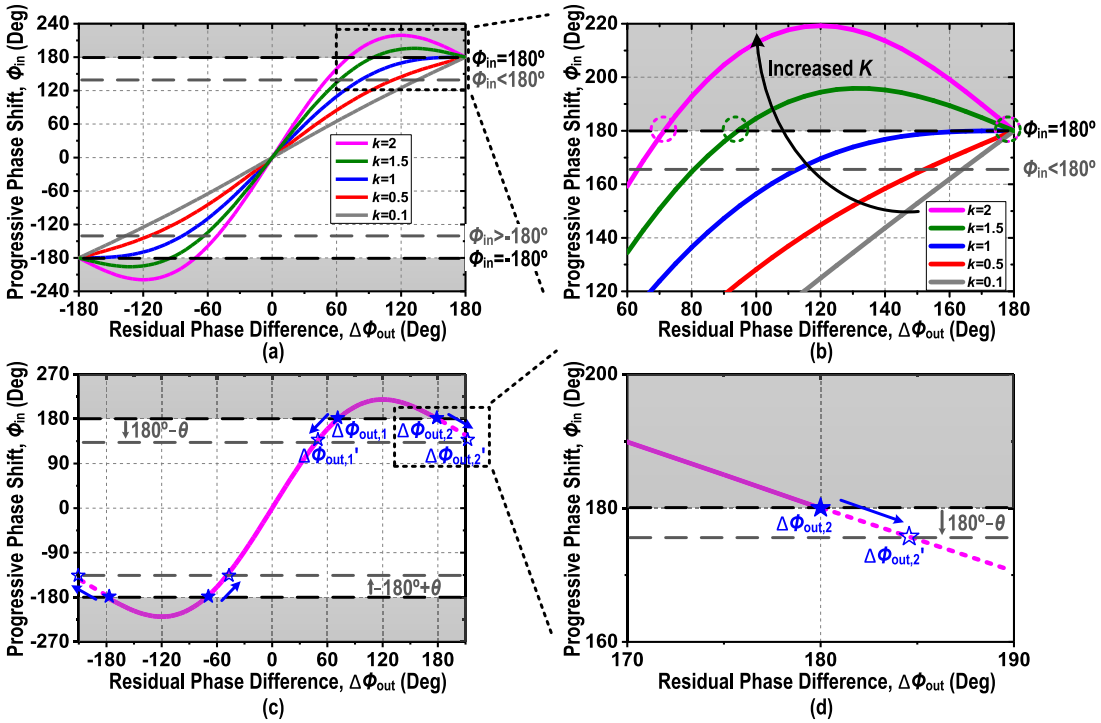

Fig. 9. (a) Progressive phase shift ϕ_{in} versus the residual phase difference $\Delta\phi_{\text{out}}$ at different k. (b) Zoomed-in view of (a) from the residual phase difference $\Delta\phi_{\text{out}} = 60°$–$180°$. (c) Perturbation analysis of the two possible solutions $\Delta\phi_{\text{out},1}$ and $\Delta\phi_{\text{out},2}$ at $\phi_{\text{in}} = \pm 180°$ for $k = 2$. (d) Zoomed-in view of (c) around $\Delta\phi_{\text{out}} = 180°$ at $k = 2$, showing the unstable solution $\Delta\phi_{\text{out},2}$.

require $3\phi_{\text{FB}}$ for phase compensation. If the same voltage-controlled phase shifters are used in path 1 and path 4, they require a control voltage of $3V_{\text{ctrl}}$, while V_{ctrl} is for path 2 and path 3, assuming that the phase shifters are in their linear regimes. A fully passive approach to generate $3V_{\text{ctrl}}$ for path 1 (and 4) can be achieved by using resistive loads with a 3:1 dividing ratio at the two rectifier outputs (Fig. 8). If V_{ctrl} is generated and regulated to the appropriate value by the negative feedback loop in path 2 and path 3, a control voltage of $3V_{\text{ctrl}}$ will be automatically generated by the resistive divider and can be used to control path 1 and path 4 (V_1 and V_4) in an open-loop manner.

D. Closed-Loop Analysis of the Nonlinear Negative Feedback Network

The large-signal closed-loop performance and the normalized array factor of the four-element beam-former are next analyzed. First, the residual output phase error $\Delta\phi_{\text{out}}$ can be expressed as

$$\begin{aligned}\Delta\phi_{\text{out}} &= \phi_{\text{in}}/(1 + G_1G_2)\\ &= \phi_{\text{in}}/[1 + (2\alpha\beta^2A^2 \sin\Delta\phi_{\text{out}}/\Delta\phi_{\text{out}})G_2]. \quad (7)\end{aligned}$$

Note that G_1 is not a fixed value, and it varies with $\Delta\phi_{\text{out}}$, i.e., the residual error phase after the compensation. Thus, the negative feedback loop is a nonlinear loop, and (7) can be simplified as

$$\Delta\phi_{\text{out}} + k \sin\Delta\phi_{\text{out}} = \phi_{\text{in}} \quad (8)$$

where $k = 2\alpha\beta^2A^2G_2$, which is the loop gain at $\phi_{\text{in}} = 0°$ when a boresight signal is received.

Since k is in a quadratic relationship with the input RF amplitude, this again indicates the loop response is a function of the input power. To examine this input power dependency and the nonlinear loop behavior, the solutions of $\Delta\phi_{\text{out}}$ in the transcendental equation (8) for a given ϕ_{in} are first analyzed. Fig. 9(a) shows the input progressive phase shift ϕ_{in} computed using (8) versus the residual output phase $\Delta\phi_{\text{out}}$ at different k. In a $\lambda/2$-spaced phased array, ϕ_{in} is confined within $\pm$ 180°, and $\Delta\phi_{\text{out}}$ is also within $\pm$ 180° by the negative feedback operation. For $-180° < \phi_{\text{in}} < 180°$, $\Delta\phi_{\text{out}}$ has only one corresponding solution for each ϕ_{in} in (8) at any k values [Fig. 9(a) and (b)]. For $\phi_{\text{in}} = \pm 180°$, i.e., when an end-fire signal is received, (8) always has a trivial solution at $\Delta\phi_{\text{out}} = \pm 180°$ regardless of k, showing that the negative feedback loop gain is zero and the self-steering is not in operation. However, if $k > 1$, (8) has one more nontrivial solution at $|\Delta\phi_{\text{out}}| < 180°$, highlighted in Fig. 9(b); based on Fig. 5(b), this solution of $|\Delta\phi_{\text{out}}| < 180°$ means that the negative feedback loop gain is nonzero and the self-steering beam-forming is still in effect even for this end-fire signal incidence. This is because the value of $\Delta\phi_{\text{out}} + k \sin\Delta\phi_{\text{out}}$ goes beyond $\pm 180°$ when $k > 1$ and then falls back to $\pm 180°$ at $\Delta\phi_{\text{out}} = \pm 180°$. On the other hand, if $k \leq 1$, $\Delta\phi_{\text{out}} + k \sin\Delta\phi_{\text{out}}$ never exceeds $\pm 180°$, and there is only one solution of $\Delta\phi_{\text{out}} = \pm 180°$ for $\phi_{\text{in}} = \pm 180°$, respectively.

A perturbation analysis is performed to analyze the stability of the two possible solutions $\Delta\phi_{\text{out}}$ for $\phi_{\text{in}} = \pm 180°$ when $k > 1$ [Fig. 9(c)]. For $\phi_{\text{in}} = 180°$, assume that a small perturbation θ ($\theta > 0$) is applied on ϕ_{in}, i.e., $\phi_{\text{in}} = 180° - \theta$. The two possible solutions $\Delta\ \phi_{\text{out},1}$ and $\Delta\phi_{\text{out},2}$ are shown in Fig. 9(c) for the case of $k = 2$. After the perturbation ($\phi_{\text{in}} = 180° - \theta$),

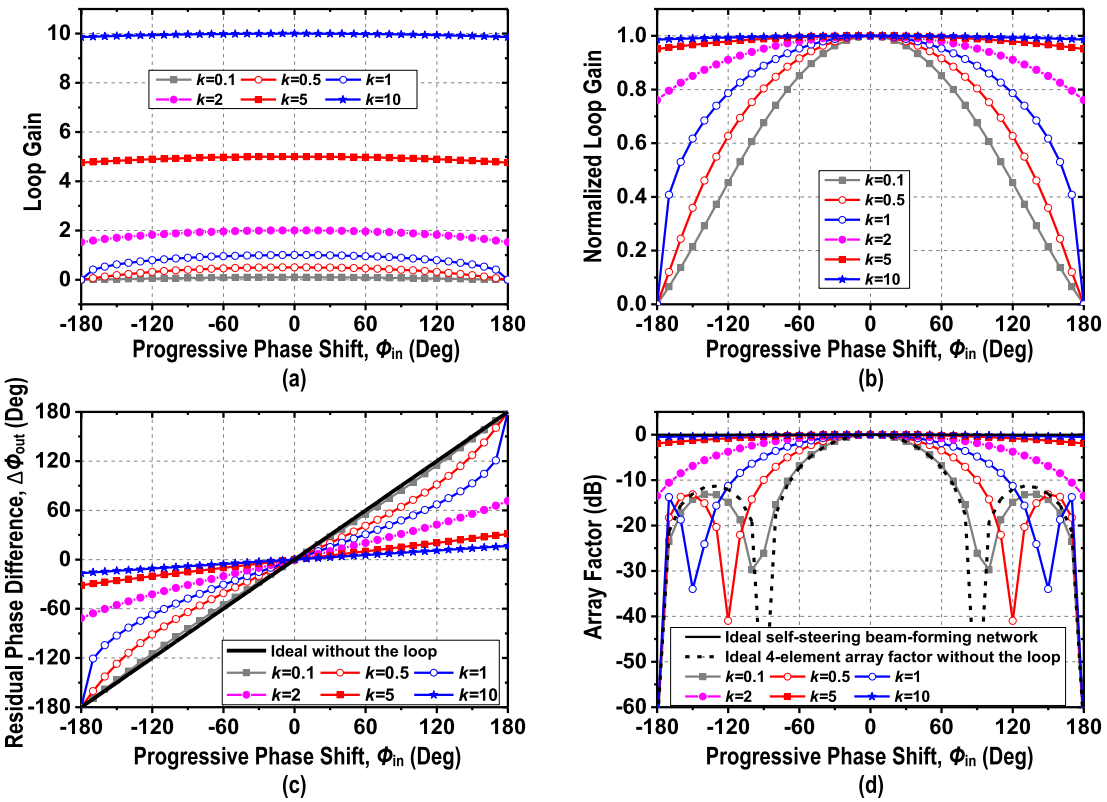

Fig. 10. (a) Simulated loop gain versus ϕ_{in}at different k. (b) Normalized loop gain versus ϕ_{in} at different k. (c) Simulated closed-loop $\Delta\phi_{out}$ between path 2 and path 3 versus ϕ_{in} at different k. (d) Simulated normalized array factor versus ϕ_{in} at different k.

$\Delta\phi_{out,1}$ becomes smaller and moves to $\Delta\phi_{out,1}$'. Thus, this $\Delta\phi_{out,1}$ is a stable solution, since $\Delta\phi_{out}$ should be smaller than 180° when $\phi_{in} < 180°$ due to the negative feedback. However, the other solution $\Delta\phi_{out,2} = 180°$ moves to a larger $\Delta\phi_{out,2}$' that exceeds 180° when $\phi_{in} < 180°$ [Fig. 9(d)]; this $\Delta\phi_{out,2}$ is not a stable solution and conflicts with the negative feedback operation. This perturbation analysis can also be applied for $\phi_{in} = -180°$, indicating that $\Delta\phi_{out} = -180°$ is not a stable solution for $k > 1$. Therefore, when $k > 1$, there is only one stable solution $|\Delta\phi_{out}| < 180°$ for $|\phi_{in}| = 180°$. This stable solution can be solved numerically based on (8) or graphically using [Fig. 9(a)]. However, for $k \leq 1$, $\Delta\phi_{out} = \pm 180°$ is the only solution and also the stable solution for $\phi_{in} = \pm 180°$, respectively.

The total large-signal loop gain and the normalized array factor are presented versus the input progressive phase difference ϕ_{in} at different k values (Fig. 10). For a given progressive phase difference ϕ_{in} of the received RF input, the residual phase error $\Delta\phi_{out}$ is calculated using (8), and the total loop gain is obtained as $G_1G_2 = (2\alpha\beta^2A^2\sin\Delta\phi_{out}/\Delta\phi_{out})G_2$. The large-signal loop gain peaks at $\phi_{in} = 0°$ and gradually decreases when ϕ_{in} approaches ±180° [Fig. 10(a)]. The normalized loop gain, i.e., the loop gain at different ϕ_{in} divided by k, is shown in Fig. 10(b). A large k ($k > 1$) always maintains a large loop gain for a given ϕ_{in} within and even at ±180°, while the normalized loop gain drops rapidly when ϕ_{in} approaches ±180° for a smaller k ($k \leq 1$), e.g., for a small input RF amplitude. Such a bifurcation behavior can be observed in Fig. 10(a), and its theoretical basis is explained in the nonlinear feedback loop analysis (Fig. 9). If $k \leq 1$, the only solution $\Delta\phi_{out}$ is ±180° for $\phi_{in} = \pm 180°$, and the resulting loop gain drops to zero based on (6) and (7). However, if $k > 1$, a nontrivial stable solution of $|\Delta\phi_{out}| < 180°$ exists for $\phi_{in} = \pm 180°$, leading to a nonzero loop gain even at $\phi_{in} = \pm 180°$ based on (6) and (7) [Fig. 5(b)]. Fig. 10(c) plots $\Delta\phi_{out}$ versus ϕ_{in} for different k values. As k becomes larger, the residual output phase error $\Delta\phi_{out}$ becomes closer to 0 for ϕ_{in} between ±180°, showing the desired phase suppression by the self-steering negative feedback loop. A smaller k ($k \leq 1$) loses the feedback control capability when ϕ_{in} approaches ±180° with the resulting $\Delta\phi_{out} \approx \phi_{in}$, while a larger k ($k > 1$) ensures a large phase suppression even at $\phi_{in} = \pm 180°$. This is also verified in the large-signal loop gain plots in Fig. 10(a) and (b).

Next, assuming that the RF input signals for the four paths have the same amplitude, the normalized array factors can be simulated versus ϕ_{in} at different k values [Fig. 10(d)]. A significant array factor improvement is achieved when k is large due to the minimized residual phase difference of the four paths even at $\phi_{in} = \pm 180°$. On the other hand, when k becomes smaller, array nulls will appear, and the array eventually degrades to a standard four-element array without self-steering compensation.

The analyses and simulations above demonstrate that our proposed all-passive self-steering beam-former achieves autonomous and substantial array factor improvement with

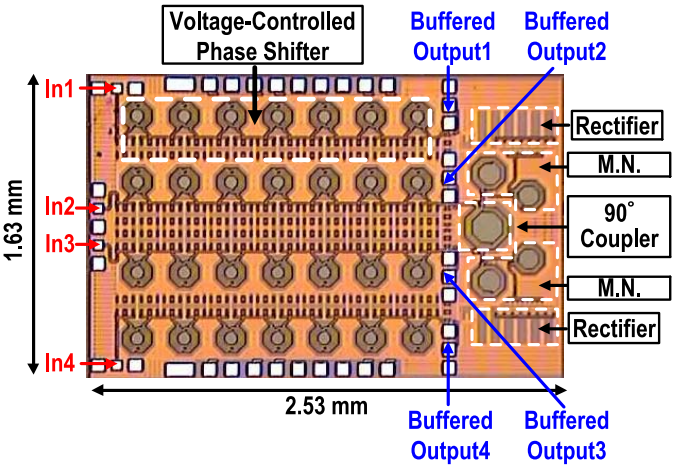

Fig. 11. Chip microphotograph.

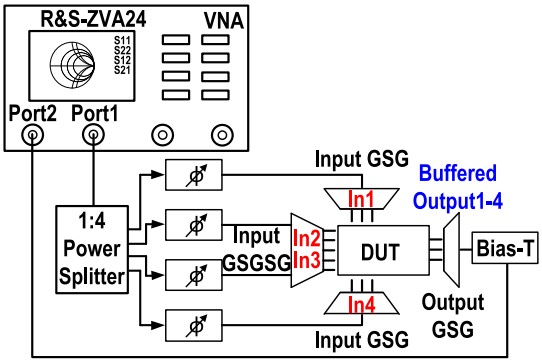

Fig. 12. Measurement setup for the closed-loop measurement.

a wide FoV over a standard four-element phased array. The nonlinear conversions between the voltage and phase signals are exploited to maximize the loop gain. *Most importantly, the proposed all-passive self-steering beam-former forms a nonlinear negative feedback that can provide a large loop gain and support self-steering operation even when receiving an end-fire signal ($\phi_{in} = \pm 180°$). This significantly expands the array FoV and cannot be realized using linear negative feedback loops.*

IV. Experimental Results

The all-passive four-element self-steering beam-former is implemented in a standard 130 nm CMOS process with an area of 1.63 mm × 2.53 mm (Fig. 11). The array measurement setup is shown in Fig. 12. A 1:4 power splitter and four phase shifters synthesize the four RF inputs to test the beam-former system. The four open-drain buffered RF outputs are sequentially probed, and the normalized array factor is calculated based on the measured amplitudes and phases of the four buffered RF outputs. The four feedback control voltages V_1–V_4 are also monitored.

The input reflection coefficients and the noise figure are first measured by direct probing. A good input matching of the four paths is achieved from 4 to 5.8 GHz with an RF input power of $P_{\text{in}} = -17$ dBm/element [Fig. 13(a)]. The measured four-path input reflection coefficients are similar at different P_{in} (Fig. 14). The averaged noise figure of the proposed circuit is measured as 9.5 dB [Fig. 13(b)], which can be compensated by the front-end LNAs.

A. Open-Loop Measurement

To evaluate the open-loop performance, the negative feedback loop is disabled by opening the switches and disconnecting the feedback voltage (Fig. 3). The measured differential DC feedback control voltage for path 1 and path 2 versus the open-loop phase error $\Delta\phi_{\text{out}}$ is shown in Fig. 15. Note that $\Delta\phi_{\text{out}} = \phi_{\text{in}}$, since the loop is open, and ϕ_{in} is the input progressive phase difference of two adjacent channels. The voltages in path 1 and path 2 exhibit a sinusoidal behavior versus $\Delta\phi_{\text{out}}$ from −180° to 180°, agreeing well with the theoretical phase-to-voltage conversion analysis (Section III-A). Moreover, the measured feedback voltage in path 1 is 3× larger than that in path 2, verifying that the 3:1 resistive divider at the rectifier output indeed creates a 3× replica control voltage. Fig. 16 shows the measured differential DC feedback voltage in path 2 versus the open-loop phase error $\Delta\phi_{\text{out}}$ at different P_{in}/element. From (5), when the input power is increased by 3 dB, the V_{ctrl} should be doubled, assuming that the rectifier is a square-law device with a constant conversion coefficient α and a constant coefficient β for the matching network. In measurements, when P_{in} is increased by 3 dB, the measured V_{ctrl} is increased by a factor of 1.9 (Fig. 16), matching well with the theoretical analysis. The small difference is possibly due to the conversion coefficient drop at a higher RF input power.

B. Closed-Loop Measurement

The measured normalized array factor of the all-passive four-element self-steering beam-former at 5 GHz is shown in Fig. 17. For an ideal self-steering beam-former, the normalized array factor should be constant at 0 dB regardless of the input progressive phase shift ϕ_{in}. On the other hand, a static four-element phased array with no self-steering compensation shows narrow beam width with two array factor nulls at $\phi_{\text{in}} = \pm 90°$, restricting the FoV. When the self-steering negative feedback loop is enabled, the proposed beam-former achieves significant array factor improvement from −180° to 180°. At $P_{\text{in}} = -17$ dBm/element, the measured normalized array factor is −2.87/−2.8 dB at +90°/−90°, showing >25 dB improvement over the null points when the feedback is disabled. The array factor also improves with a higher RF input power due to the increased feedback loop gain. The measured array factor reaches −0.15/−0.14 dB at +90°/−90° with $P_{\text{in}} = -8$ dBm/element. Moreover, a higher RF input power also substantially improves the array factor even at $\phi_{\text{in}} = \pm 180°$, benefiting from the nonlinear feedback loop operation of the proposed self-steering beam-former.

On the other hand, decreasing the RF input power weakens the array loop gain. Array factor nulls start to appear, and the array performance is eventually degraded to a static four-element phased array without any compensation, meaning that the feedback loop gain gradually becomes

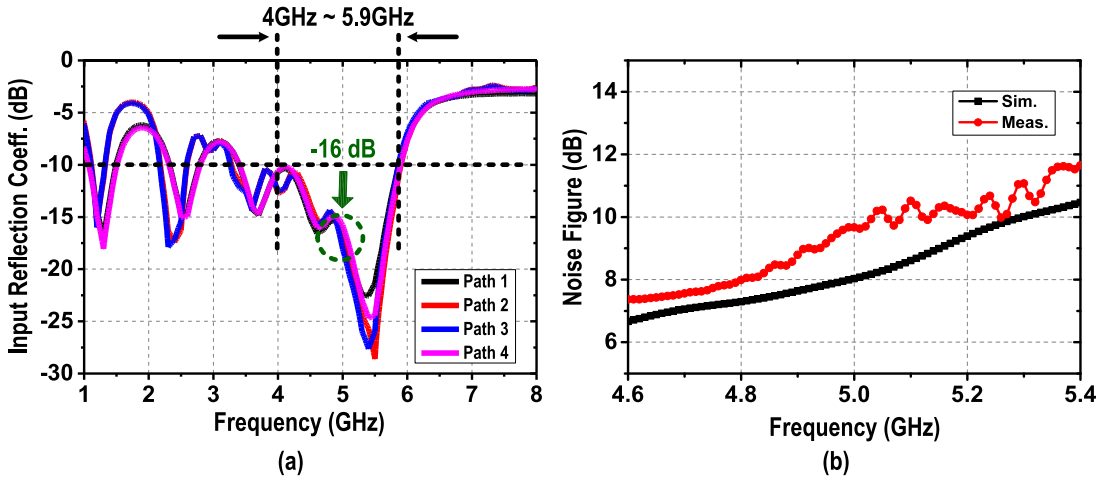

Fig. 13. (a) Measured input reflection coefficient of paths 1–4 with $P_{\text{in}} = -17$ dBm/element. (b) Simulated and measured noise figure of the proposed circuit.

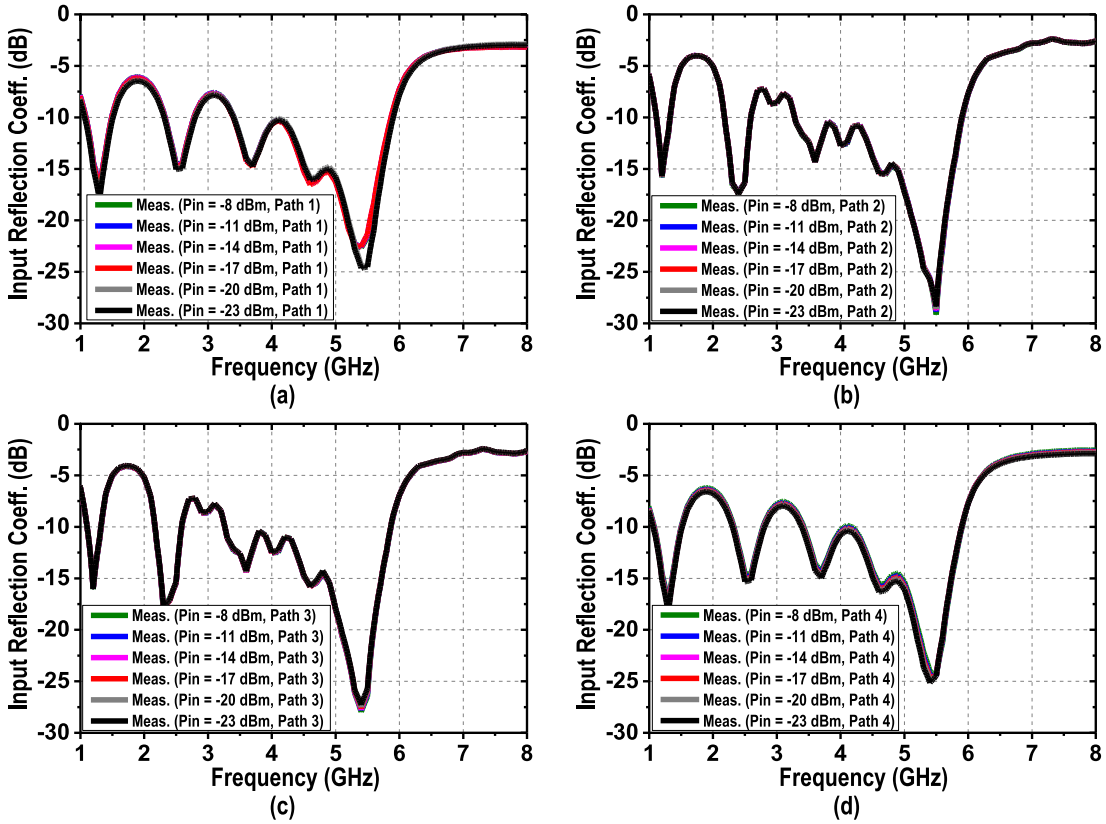

Fig. 14. Measured input reflection coefficient of (a) path 1, (b) path 2, (c) path 3, and (d) path 4 at different RF input power levels (P_{in} per element).

zero. Fig.18 shows the measured array factor at ±90° with and without negative feedback versus P_{in} per element. The negative feedback loop shows substantial effect for $P_{\text{in}} > -29$ dBm/element. Fig. 19 shows the Monte Carlo simulation result based on 200 samples and a measured normalized array factor of our proposed passive self-steering beam-former circuit with $P\text{in} = -17$ dBm/element at 5 GHz. The Monte Carlo simulations use the default Monte Carlo models in the GlobalFoundries GFUS 8RF design kit, including both corner variations and device mismatches. The error bar of the simulated normalized array factor equals one standard deviation.

The measurements (three measurement curves) are based on three independent samples and thus include the random variations and mismatches in practice. Based on our Monte Carlo simulations, the variation of the simulated normalized array factor is within 0.8 dB, which shows the robustness of the proposed design. Moreover, the measured normalized array factors for the three independent samples closely match the Monte Carlo simulations, verifying that the process variations and device mismatches will not cause significant degradation in array factor in practice.

To characterize the FoV and bandwidth of the proposed beam-former, the FoV is defined by the input progressive

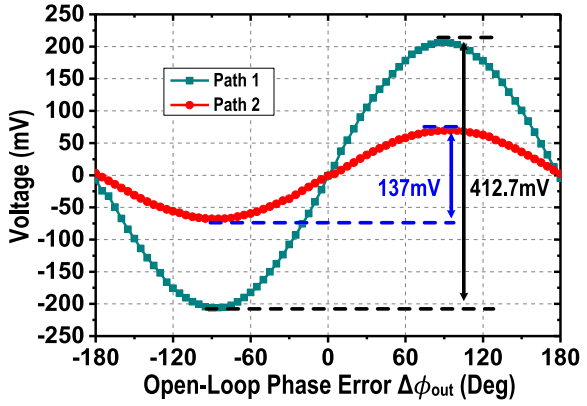

Fig. 15. Measured feedback control voltage difference across varactors in path 1 and path 2 versus the open-loop phase error $\Delta\phi_{\text{out}} = \phi_{\text{in}}$ with $P_{\text{in}} = -17$ dBm/element at 5 GHz.

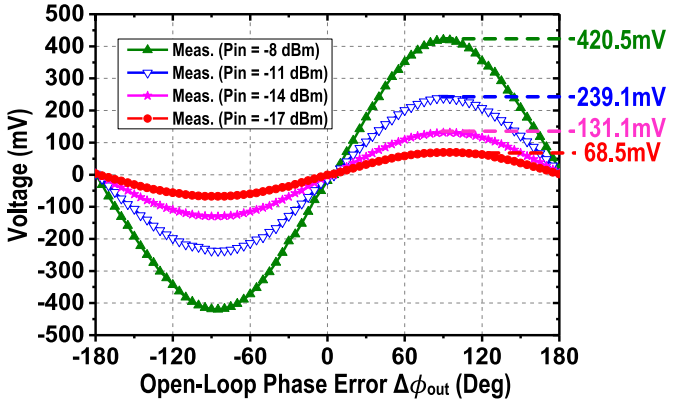

Fig. 16. Measured feedback control voltage difference across varactors in path 1 and path 2 versus the open-loop phase error $\Delta\phi_{\text{out}} = \phi_{\text{in}}$ with different P_{in}/element at 5 GHz.

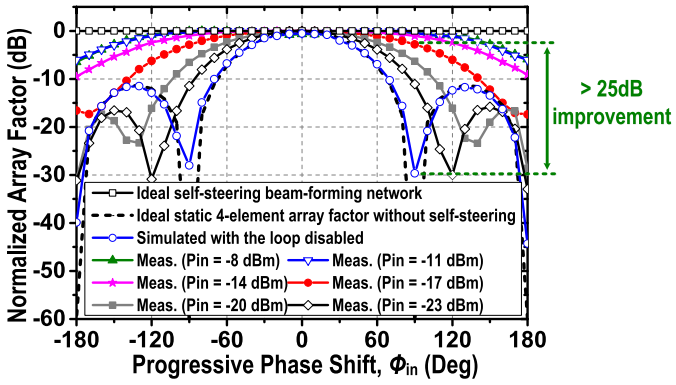

Fig. 17. Measured normalized array factor of the four-element array versus ϕ_{in} with different P_{in} per element at 5 GHz.

phase shift ϕ_{in} range, within which the normalized array factor is better than -6 dB. The reason to choose -6 dB is that a four-element phased array offers $10 \times \log 4 = 6$ dB array gain at 0° incidence compared with a single-element receiver. Within the FoV defined by this criterion, the four-element phased array maintains its array gain advantage over single-element operation. At 5 GHz, the measured FoV is from $-120°$ to $+120°$ with $P_{\text{in}} = -17$ dBm/element and from $-180°$ to $+180°$ with $P_{\text{in}} = -11$ dBm/element (Fig. 20), showing a very wide and consistent FoV for all three

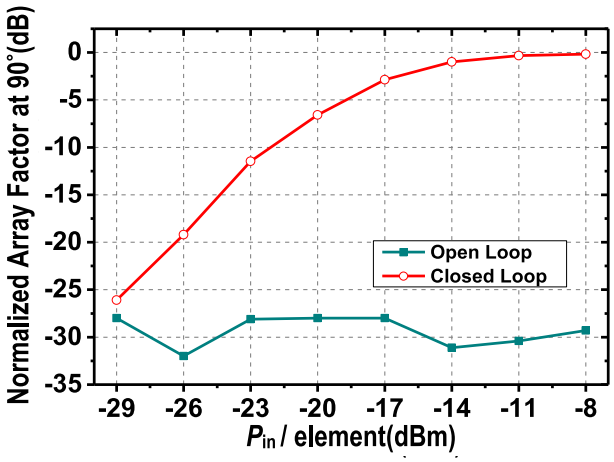

Fig. 18. Measured normalized array factor versus P_{in} per element with $\phi_{\text{in}} = 90°$ at 5 GHz.

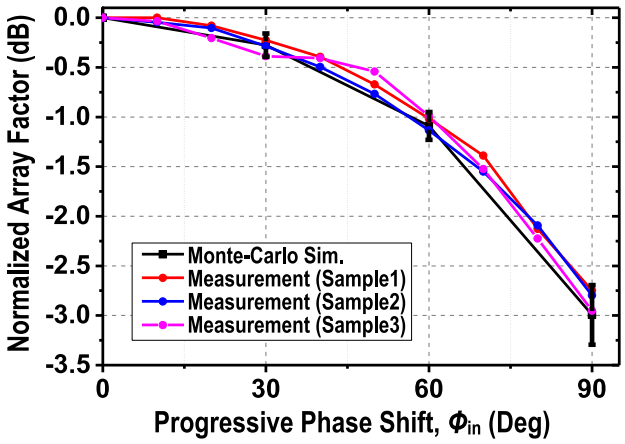

Fig. 19. Monte Carlo simulation result and measured normalized array factor of the proposed passive self-steering beam-former circuit with $P_{\text{in}} = -17$ dBm/element at 5 GHz for three independent chip samples. The highly consistent results show the robustness of the design.

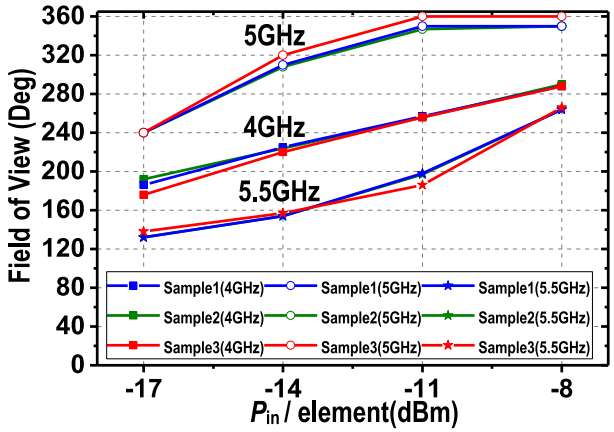

Fig. 20. Measured FoV versus P_{in}/element at 4, 5, and 5.5 GHz for three independent beam-former chip samples.

independent samples. Wide FoV is also achieved at other frequencies (4 and 5.5 GHz). The measured normalized array factors at different frequencies and different input power levels are summarized in Fig. 21a–Fig. 21c. The proposed all-passive self-steering beam-former achieves a high-performance array factor enhancement from 4 to 5.5 GHz.

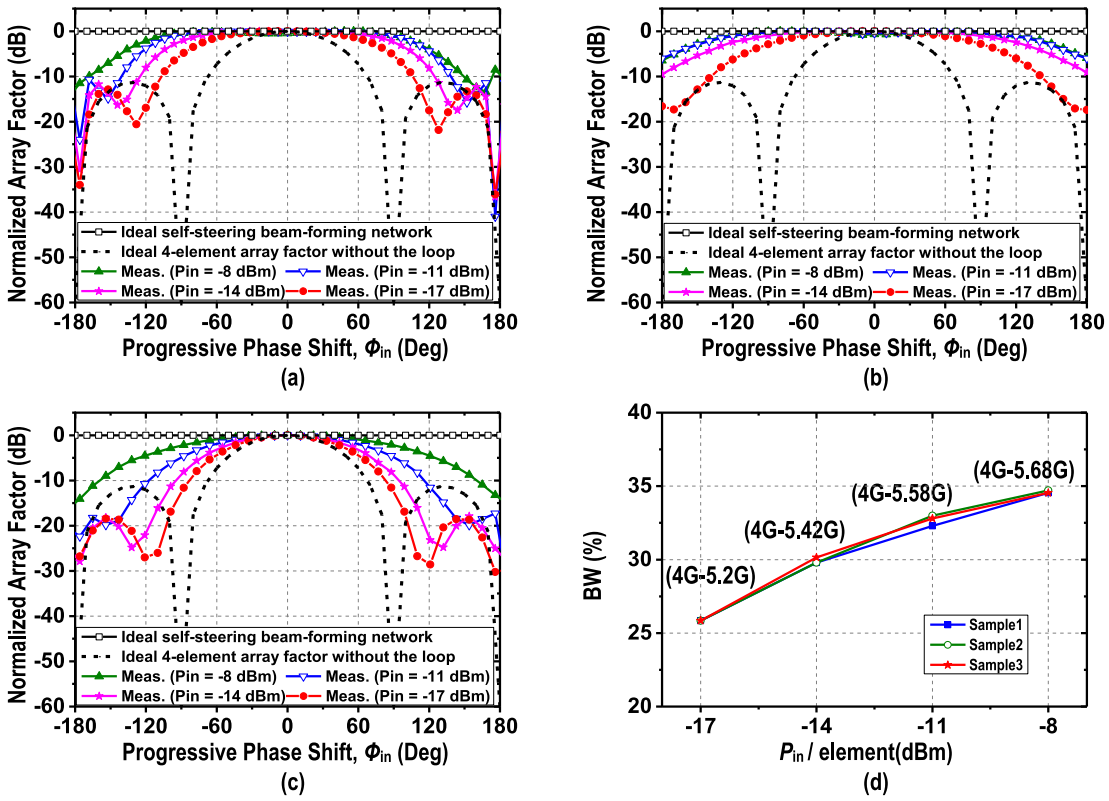

Fig. 21. Measured normalized array factor of the four-element array versus ϕ_{in} with different P_{in}/element at (a) 4, (b) 5, and (c) 5.5 GHz. (d) Measured fractional bandwidth versus different input powers for three independent beam-former chip samples.

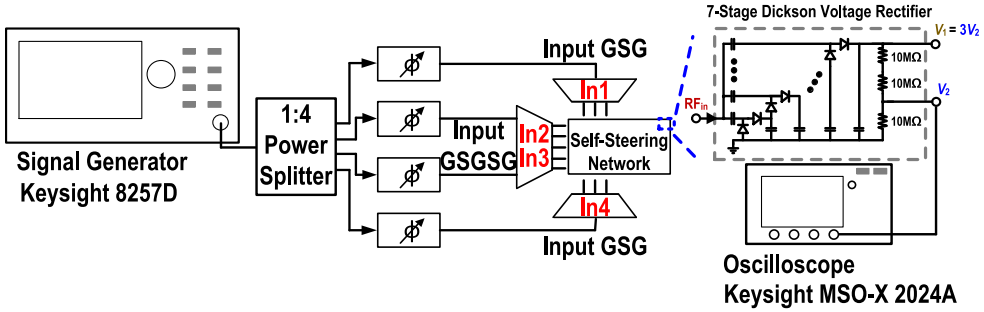

Fig. 22. Measurement setup for the system response time measurement.

The self-steering beam-former fractional bandwidth is defined as the frequency range, within which the array FoV is larger than 180° (±90°) for a given RF input power. Based on the measurements, the fractional bandwidth versus the input power for three independent samples is summarized in Fig. 21(d). At −17 dBm/element input power, the measured fractional bandwidth is 26%, which is expanded to 35% for −8 dBm/element, demonstrating a broadband operation.

C. Time-Domain Response Measurement

The time-domain response of a self-steering beam-former is critical, since it governs how fast the system can perform beam-forming in response to the onset of an input or beam-tracking to a varying input, i.e., a moving source target. The time-domain response measurement setup is shown in Fig. 22. The input RF signal ($P_{in} = -17$ dBm/element) is generated by a vector signal generator (Keysight 8257D) with an OOK modulation, and the input progressive phase shift ϕ_{in} is generated by the off-chip phase shifters to synthesize the incident wave for the self-steering beam-former chip. The time-domain response is measured by monitoring the DC feedback voltage on a real-time oscilloscope (Keysight MSO-X 2024A). On the beam-former IC, each DC feedback voltage node from the rectifiers is connected to 14 differential varactors in the phase shifters with a total capacitive loading of 168 pF, which, together with the resistive load (∼30 MΩ), forms the dominant pole of the negative feedback loop. Fig. 23(a) shows the measured time-domain waveform of the DC feedback voltage at $\phi_{in} = 90°$, showing a measured time constant of 3 ms. The measured time constant versus ϕ_{in} is summarized in Fig. 23(b), showing a similar time

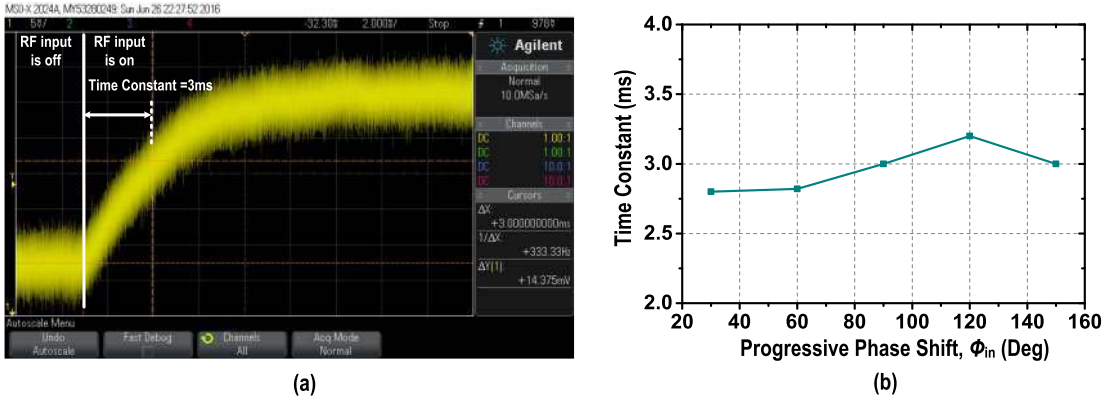

Fig. 23. (a) Measured time-domain response of the DC feedback control voltage V_2 with −17 dBm/element at 5 GHz for $\phi_{\text{in}} = 90°$. (b) Measured time constant versus ϕ_{in} with −17 dBm/element at 5 GHz.

TABLE I

PERFORMANCE SUMMARY AND COMPARISON WITH STATE-OF-THE-ART BEAM-FORMERS

	Self-Steering (No External Controls)	Element No.	Freq. (GHz)	BW	DC Power (mW)	FoV‡	Normalized Array Factor versus Input Progressive Phase Shift ϕ_{in}	Topology	Area (mm^2)	Tech.
[9]	No	2	11.2	N/A	36	±120°	N/A	ILOA	1.2 (with pads)	180nm CMOS
[10]	No	3	2.68-2.72	1.5%	725*	-28°~+39°	N/A	ILCOA	N/A	Not Fully Integrated
[8]	No	4	42.8-49.5	14.5%	85	±90°	N/A	ILOA	2.8 (core area)	65nm CMOS
[5]	Yes	2	1.425	N/A	430*	±155°	N/A	Open Loop Phase Detection + Feedforward Phase Correction	N/A	Not Fully Integrated
[6]	Yes	4	6.5	N/A	565*	-90°~+127°	N/A	Power Detector + DSP	N/A	Not Fully Integrated
[7]	Yes	4	7.4-9.4	23.8%	143	±100°	-3dB@60°/-7dB@90°**	COA + CPLL	3.5 (with pads)	45nm CMOS SOI
This Work	**Yes**	**4**	**4-5.68**	**34.7%**	**0**	**±120°† ±180°††**	**-1.1dB@60°/ -2.87dB@90°† -0.1dB@60°/ -0.15dB@90°/ -5.9dB@180°††**	**All-Passive Nonlinear Negative Feedback Loop**	**4.1 (with pads)**	**130nm CMOS**

* Estimated DC power consumption

**Estimated based on the measurement figures in [7]

† P_{in} = -17dBm/element at 5GHz

†† P_{in} = -8dBm/element at 5GHz

‡ The FoV is defined by the input progressive phase shift ϕ_{in} range, within which the normalized array factor is better than -6dB for the proposed circuit.

constant over a wide FoV. The proposed all-passive self-steering beam-former achieves an acquisition time constant of several milliseconds, which is similar to the active self-steering beam-formers and is fast enough for many phased array beam-forming applications [23]–[25].

The proposed all-passive self-steering beam-former is compared with the state-of-the-art active designs in Table I. It demonstrates superior performance, including broad bandwidth, wide FoV, and large array factor improvement, all with zero DC power consumption.

V. Conclusion

An all-passive negative feedback network is proposed to serve as a broadband and wide FoV self-steering beam-former with zero DC power consumption for a phased-array receiver. A four-element proof-of-concept design at 5 GHz is demonstrated and achieves large array factor improvement over wide bandwidth and FoV even at μW-level RF inputs. The proposed all-passive beam-former operates at zero DC power and outperforms reported state-of-the-art active designs.

References

[1] H. Wang *et al.*, "A tunable concurrent 6-to-18GHz phased-array system in CMOS," in *IEEE MTT-S Int. Microw. Symp. Dig.*, Jun. 2008, pp. 387–390.

[2] X. Guan, H. Hashemi, and A. Hajimiri, "A fully integrated 24-GHz eight-element phased-array receiver in silicon," *IEEE J. Solid-State Circuits*, vol. 39, no. 12, pp. 2311–2320, Dec. 2004.

[3] T. Yu and G. M. Rebeiz, "A 22–24 GHz 4-element CMOS phased array with on-chip coupling characterization," *IEEE J. Solid-State Circuits*, vol. 43, no. 9, pp. 2134–2143, Sep. 2008.

[4] L. D. DiDomenico and G. M. Rebeiz, "Digital communications using self-phased arrays," *IEEE Trans. Microw. Theory Techn.*, vol. 49, no. 4, pp. 677–684, Apr. 2001.

[5] G. S. Shiroma, R. Y. Miyamoto, and W. A. Shiroma, "A full-duplex dual-frequency self-steering array using phase detection and phase shifting," *IEEE Trans. Microw. Theory Techn.*, vol. 54, no. 1, pp. 128–134, Jan. 2006.

[6] J. M. Akagi, A. Zamora, M. K. Watanabe, and W. A. Shiroma, "A self-steering array using power detection and phase shifting," in *IEEE MTT-S Int. Microw. Symp. Dig.*, Jun. 2008, pp. 1325–1328.

[7] A. K. Gupta and J. F. Buckwalter, "A self-steering receiver array using jointly coupled oscillators and phased-locked loops," *IEEE Trans. Microw. Theory Techn.*, vol. 62, no. 3, pp. 631–644, Mar. 2014.

[8] L. Wu, A. Li, and H. C. Luong, "A 4-path 42.8-to-49.5 GHz LO generation with automatic phase tuning for 60 GHz phased-array receivers," *IEEE J. Solid-State Circuits*, vol. 48, no. 10, pp. 2309–2322, Oct. 2013.

[9] Y. T. Lo and J. F. Kiang, "Comparison of injection-locked and coupled oscillator arrays for beamforming," *IEEE Trans. Microw. Theory Techn.*, vol. 63, no. 4, pp. 1353–1360, Apr. 2015.

[10] S. H. Yan and T. H. Chu, "A beam-steering antenna array using injection locked coupled oscillators with self-tuning of oscillator free-running frequencies," *IEEE Trans. Antennas Propag.*, vol. 56, no. 9, pp. 2920–2928, Sep. 2008.

[11] M. Tabesh *et al.*, "A 65nm CMOS 4-element sub-34mW/element 60GHz phased-array transceiver," in *IEEE Int. Solid-State Circuits Conf. (ISSCC) Dig. Tech. Papers*, Feb. 2011, pp. 166–167.

[12] R. Y. Miyamoto and T. Itoh, "Retrodirective arrays for wireless communications," *IEEE Microw. Mag.*, vol. 3, no. 1, pp. 71–79, Mar. 2002.

[13] S. Lim, K. M. K. H. Leong, and T. Itoh, "Adaptive power controllable retrodirective array system for wireless sensor server applications," *IEEE Trans. Microw. Theory Techn.*, vol. 53, no. 12, pp. 3735–3743, Dec. 2005.

[14] Y. Li and V. Jandhyala, "Design of retrodirective antenna arrays for short-range wireless power transmission," *IEEE Trans. Antennas Propag.*, vol. 60, no. 1, pp. 206–211, Jan. 2012.

[15] A. Massa, G. Oliveri, F. Viani, and P. Rocca, "Array designs for long-distance wireless power transmission: State-of-the-art and innovative solutions," *Proc. IEEE*, vol. 101, no. 6, pp. 1464–1481, Jun. 2013.

[16] M.-Y. Huang, T. Chi, and H. Wang, "A 5GHz all-passive negative feedback network for RF front-end self-steering beam-forming with zero DC power consumption," in *Proc. IEEE RF Integr. Circuits Symp. (RFIC)*, May 2016, pp. 91–94.

[17] J. M. Rabaey *et al.*, "PicoRadios for wireless sensor networks: The next challenge in ultra-low power design," in *IEEE Int. Solid-State Circuits Conf. (ISSCC) Dig. Tech. Papers*, Feb. 2002, pp. 200–201.

[18] Y. Zhang *et al.*, "A batteryless 19 μW MICS/ISM-band energy harvesting body sensor node SoC for ExG applications," *IEEE J. Solid-State Circuits*, vol. 48, no. 1, pp. 199–213, Jan. 2013.

[19] D. Yoon, D. Sylvester, and D. Blaauw, "A 5.58 nW 32.768 kHz DLL-assisted XO for real-time clocks in wireless sensing applications," in *IEEE Int. Solid-State Circuits Conf. (ISSCC) Dig. Tech. Papers*, Feb. 2012, pp. 366–367.

[20] R. E. Barnett, J. Liu, and S. Lazar, "A RF to DC voltage conversion model for multi-stage rectifiers in UHF RFID transponders," *IEEE J. Solid-State Circuits*, vol. 44, no. 2, pp. 354–370, Feb. 2009.

[21] J. S. Park and H. Wang, "A passive quadrature generation scheme for integrated RF systems," in *IEEE MTT-S IWS Dig. Tech. Papers*, Apr. 2013, pp. 1–4.

[22] F. Wang and H. Wang, "A broadband compact low-loss 4×4 butler matrix in CMOS with stacked transformer based quadrature couplers," in *IEEE MTT-S Int. Microw. Symp. Dig.*, May 2016, pp. 1–4.

[23] B. S. Leibowitz, B. E. Boser, and K. S. J. Pister, "A 256-element CMOS imaging receiver for free-space optical communication," *IEEE J. Solid-State Circuits*, vol. 40, no. 9, pp. 1948–1956, Sep. 2005.

[24] R. Ebelt *et al.*, "Cooperative indoor localization using 24-GHz CMOS radar transceivers," *IEEE Trans. Microw. Theory Techn.*, vol. 62, no. 9, pp. 2193–2203, Sep. 2014.

[25] S. S. Ahmed, A. Schiessl, and L.-P. Schmidt, "A novel fully electronic active real-time imager based on a planar multistatic sparse array," *IEEE Trans. Microw. Theory Techn.*, vol. 59, no. 12, pp. 3567–3576, Dec. 2011.

Min-Yu Huang (S'14) received the B.S. degree (with highest Hons.) in electrical engineering and computer science from National Tsing Hua University (NTHU), Hsinchu, Taiwan, in 2013. He is currently pursuing the Ph.D. degree in electrical engineering with the Georgia Institute of Technology, Atlanta, GA, USA.

His current research interests include RF/mm-wave integrated circuits and systems.

Mr. Huang was a recipient of the IEEE Radio Frequency Integrated Circuits Symposium Best Student Paper Award (second place) in 2016, the Scholarship of the Outstanding Student in Engineering from the Chinese Institute of Engineers, Taiwan, in 2013, and the NTHU EECS Outstanding Student Scholarship in 2012.

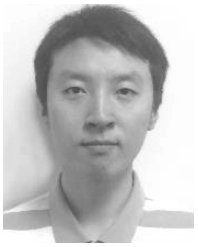

Taiyun Chi (S'11) received the B.S. degree (with highest Hons.) from the University of Science and Technology of China, Hefei, China, in 2012. He is currently pursuing the Ph.D. degree in electrical engineering with the Georgia Institute of Technology, Atlanta, GA, USA.

His current research interests include millimeter-wave/terahertz integrated circuits, and integrated biomedical sensors and actuators.

Mr. Chi was a recipient of the 2016 Microwave Theory and Techniques Society Graduate Fellowship for Medical Applications, the Analog Devices Inc., Outstanding Student Designer Award in 2015, the Texas Instruments CICC Student Scholarship Award in 2014, the Georgia Tech GEDC Fellowship in 2012, and the USTC Guo Moruo Presidential Scholarship in 2012. He was a co-recipient of the IEEE SENSORS Best Live Demo Award (second place) in 2016, and the IEEE Radio Frequency Integrated Circuits Symposium Best Student Paper Award (second place) in 2016.

Fei Wang (S'14) received the B.S. degree in microelectronics from Fudan University, Shanghai, China, in 2014. He is currently pursuing the Ph.D. degree in electrical engineering with the Georgia Institute of Technology, Atlanta, GA, USA.

His research interests include mixed-signal, RF, and millimeter-wave integrated circuits and systems for wireless communications.

Mr. Wang was the recipient of the Georgia Tech ECE Graduate Fellowship in 2014, the 1st Prize in Shanghai Undergraduate Mathematical Competition in 2012, and the Tencent Innovation Scholarship at Fudan University in 2012.

Hua Wang (M'05–SM'15) received the M.S. and Ph.D. degrees in electrical engineering from the California Institute of Technology, Pasadena, CA, USA, in 2007 and 2009, respectively.

He was with Intel Corporation, and Skyworks Solutions. He joined the School of Electrical and Computer Engineering, Georgia Institute of Technology, Atlanta, GA, USA, as an Assistant Professor in 2012. His current research interests include mixed-signal, RF, and millimeter-wave integrated circuits and systems for wireless communication, radar, imaging, and bioelectronics applications.

Dr. Wang is a member of Sigma Xi, the IEEE Solid-State Circuits Society, the IEEE Microwave Theory and Techniques Society, the IEEE Circuits and Systems Society, and the IEEE Engineering in Medicine & Biology Society. He was a recipient of the National Science Foundation CAREER Award in 2015, the 2016 Georgia Tech Sigma Xi Young Faculty Award, the 2014 DURIP Award, the Georgia Tech ECE Outstanding Junior Faculty Member Award in 2015, and the Lockheed Dean's Excellence in Teaching Award in 2015. He currently holds the Demetrius T. Paris Junior Professorship of the School of Electrical and Computer Engineering. His research group Georgia-Tech Electronics and Micro-System Laboratory has won multiple Student Paper Awards and Student Designer Awards, including the IEEE RFIC Best Student Paper Awards in 2014 (first place) and 2016 (second place), the IEEE CICC Best Student Paper Awards in 2015, the 2016 IEEE Microwave Magazine Best Paper Award, and three times the IEEE CICC Best Student Paper Finalists. He served as the Chair of the Atlanta's IEEE CAS/SSCS joint chapter, which won the IEEE SSCS Outstanding Chapter Award in 2014. He is an Associate Editor of the IEEE MICROWAVE AND WIRELESS COMPONENTS LETTERS. He is currently a Technical Program Committee Member of the IEEE Radio Frequency Integrated Circuits Symposium, the IEEE Custom Integrated Circuits Conference, the IEEE Biopolar/BiCMOS Circuits and Technology Meeting, the IEEE Sensors Conference, and the IEEE Biomedical Circuits and Systems Conference.